Journal of Molecular Liquids 381 (2023) 121783

Contents lists available at ScienceDirect

Journal of Molecular Liquids

journal homepage: www.elsevier.com/locate/molliq

Photophysical and photochemical properties of 3-hydroxyflavone in ethanol solution: Implicit *vs* explicit solvent models

Samuel Frutos-Puerto [a], M. Jesús Colín [a], Jose C. Corchado [a,b], M. Luz Sánchez [a,b], M. Elena Martín [a,b], Manuel A. Aguilar [a,b]

[a] Área de Química-Física, Facultad de Ciencias, Universidad de Extremadura, Spain
[b] Instituto de Computación Científica Avanzada (ICCAEx), Universidad de Extremadura, Avda. de Elvas, 06006 Badajoz, Spain

ARTICLE INFO

Article history:
Received 23 December 2022
Revised 27 March 2023
Accepted 31 March 2023
Available online 4 April 2023

ABSTRACT

Photophysical and photochemical properties of 3-hydroxyflavone in gas-phase and solution were studied using implicit (Polarizable Continuum Model, PCM) and explicit solvent (Averaged Solvent Electrostatic Potential from Molecular Dynamics calculations, ASEP/MD) models. The conformational equilibrium in the excited state between the normal (N*) and tautomeric (T*) forms and their absorption and fluorescence spectra was studied with Time-Dependent Density Functional Theory (TD-DFT) and three different functionals. The calculated transitions are in good agreement with the spectroscopic data. It was found that solvent effects on the absorption and fluorescence spectral bands are negligible. Still, they can modify appreciably the relative stability of the N* minimum with respect to the Franck-Condon position, which affects the kinetics of the reaction. This fact, together with the increase in the barrier height in protic solvents, permits us to explain the reduction of the emission signal from T* and the increase of the N* signal in ethanol solution.

1. Introduction

Flavonols [1] and more specifically the 3-hydroxyflavone (3–HF) and related compounds have received much attention [2,3,4,5,6,7,8,9] over the last few decades as they serve as model systems to study excited state intramolecular proton transfer (ESIPT) [10,11,12,13,14,15,16,17]. When the ESIPT process takes place in a flavonol, such as the 3–HF molecule, N form in Fig. 1, the proton is transferred from the hydroxyl to the carbonyl group, tautomeric form T in Fig. 1, while the system remains in the excited state. The frequency and intensity of the emission bands (from the initial state N* or from the tautomer T*) can be tuned by a suitable choice of substituents and solvents, being able in some cases to observe dual fluorescence. This feature, together with the large Stokes shift shown by flavonols, explains the important role of these compounds as fluorescent probes, fluorescent sensors, organic light emitting diodes, etc [17–21].

In flavonols with electron-donor or electron-acceptor groups, electron transitions trigger important charge fluxes, therefore they display large hypsochromic and bathochromic shifts. Conversely, absorption and emission spectra of 3–HF are hardly dependent on the solvent polarity, although the relative intensity of the bands, I_{N^*}/I_{T^*}, is largely dependent on the solvent nature [3,22]. Thus, for instance, in cyclohexane and toluene only the emission from T* is observed. As the solvent polarity increases, so does the signal from N*, in such a way that in acetonitrile the ratio I_{N^*}/I_{T^*} rises to 0.27. In proton-donor solvents the signal from T* decreases appreciably while the intensity of N* increases [4]. From a kinetic point of view, cryogenic experiments with 3–HF have shown that the ESIPT reaction is barrierless and takes place in less than a picosecond [13,23]. In solution, time constants of 35–240 fs have been estimated using different experimental techniques and solvents. For instance, Ameer-Beg et al. found that 35 fs would be required to produce the keto form in solvents such as methylcyclohexane (non-polar) or acetonitrile (aprotic). This time rises to 60 fs in ethanol, a protic solvent [24].

The increase of the relative intensity of the N* band in proton-donor solvents has been linked to the stabilization of an alternate conformation (form A in Fig. 1) where an intermolecular hydrogen bond (HB) is formed between the hydroxylic hydrogen of 3–HF and the solvent [22]. For obvious reasons, in this alternate form, where the hydroxyl group is rotated, the ESIPT reaction is not possible, which would explain both the reduction of the T* signal and the increase of the N* signal. However, to the best of our knowledge, no theoretical study has aimed to determine the relative stability of both forms (N *vs* A). We will attempt to clarify this point in the present study.

https://doi.org/10.1016/j.molliq.2023.121783
0167-7322/

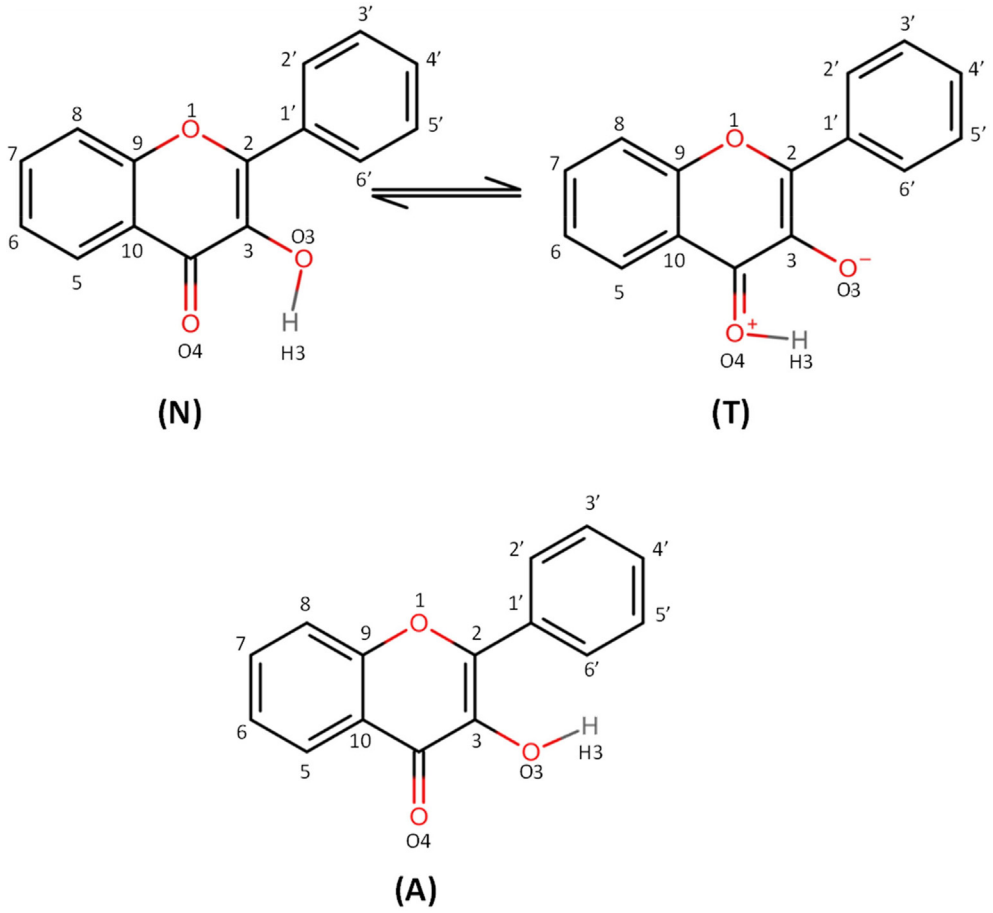

Fig. 1. Atom numbering of 3–HF normal (**N**), tautomeric (**T**) forms, and alternate (**A**) conformation.

As for the reduction of the rate constant in proton-donor solvents the mechanism is neither clear nor easy to study. It is necessary to consider several aspects such as: bulk and specific solvent effects, equilibrium and non-equilibrium solvation, or the contribution of tunneling. Both bulk and specific solvent effects seem to increase the barrier height, although the relative importance of these contributions is not clear. In this paper we aim to address some of these points.

Several theoretical studies have examined the spectroscopy and ESIPT reactivity of 3–HF both in gas phase and in solution. Most of these studies used solvent implicit continuum models [25,26] or explicitly included one or two solvent molecules. Salaeh et al. [8] used 25 QM/MM trajectories to describe the dynamics of the reaction. It was found that 80% of trajectories do suffer ESIPT reaction during the time of simulation. Even though all the studies predicted a small barrier height (2–3 kcal/mol) for the ESIPT reaction, some discrepancies were found in the reaction free energy values. Thus, Casadesús [27] using CASPT2//CASSCF, found values close to 8 kcal/mol whereas most TD-DFT studies found values close to 3–4 kcal/mol [28]. Both the TD-DFT and the CASPT2 methods seem to offer an adequate description of both the absorption and emission spectra of 3–HF.

The main goal of this paper is to compare the performance of both implicit and explicit solvent models in describing the spectroscopy of the system and the kinetics of the reaction in the excited state. We have focused on the location of the different critical points (minima, transition state, Frank-Condon points, etc.) on the free energy surface of the excited state. The distinctive features of our study are: firstly, the use of a QM/MM method that takes advantage of mean field approximation and permits to analyze the changes in the solvent structure accompanying excitation and the ESIPT reaction; secondly, the calculation of free energy differences between the alternate (A) and normal (N) forms in the ground state and between the normal (N) and tautomeric (T) isomers in the excited state; finally, the study of the kinetics of the reaction and the effect of tunneling on the rate constant.

The rest of the paper is organized as follows: Section II introduces the theoretical methods used along the study. The focus is on describing the Averaged Solvent Electrostatic Potential/Molecular Dynamics (ASEP/MD) method and on how the rate constants and tunneling corrections are calculated. Section III presents the main results obtained. For the sake of completeness, and to make the analysis of the in-solution results easier, the calculated gas-phase results are also presented, although they do not significantly differ from most of the results found in the literature. The main part of this section is devoted to the analysis of the in-solution results. We focus on the comparison between implicit and explicit solvent models, the analysis of the changes in the solvent structure in the critical points, the description of the excited state free energy surface, and the calculation of the rate constant and the tunneling effect correction. Finally, Section IV presents the main conclusions.

1.1. Computational methods and details

Ground and excited state properties of normal (**N**) and tautomeric (**T**) forms of 3–HF were studied both in gas phase and in ethanol solution using Density Functional Theory (DFT) and Time Dependent Density Functional Theory (TD–DFT). Fig. 1 displays the atom numbering of both N and T structures, as well as the A

form. Two hybrids (B3LYP [29] and PBE0 [30]) and one long-range corrected hybrid functional (CAM-B3LYP [31]), using the 6-311 +G** basis set, have been used. Previous studies have proven that the TD-DFT theory and B3LYP functional with triple-zeta valence basis set with polarization functions are suitable to describe electronic and photophysical properties as well as the proton transfer (PT) processes of ESIPT in molecules [8,32,33,34,35,36], so this comparison will allow us to analyze the accuracy of the widely used PBE0 and CAM-B3LYP functionals. Quantum chemical calculations were made with the Gaussian 16 program package [37]).

Solvent effects were described using two different methods: Polarizable Continuum Method (PCM [38,39,40]) and ASEP/MD [41,42]. The former is an implicit solvent model that describes the solvent as a continuum dielectric. This method has been widely used and has demonstrated its utility and versatility in a multitude of chemical systems and processes. The latter method is an explicit solvent model developed in our laboratory that combines quantum mechanics calculations in the description of the solute with a detailed description of the solvent through molecular dynamics simulations. Both methods permit to describe equilibrium and non-equilibrium (frozen solvent) solvation [43,44]. In the equilibrium version the solvent is assumed to be in equilibrium with the current charge distribution of the solute; in contrast, in the non-equilibrium version the solvent is equilibrated, total or partially, with the charge distribution that the solute had at a previous stage of the calculation, usually the charge distribution of the initial state before the absorption or emission process has taken place. The study of the influence of the solvent on the electronic spectrum of molecules in solution using PCM and TD-DFT methods can be carried out according to two schemes known as linear response (LR [45,46]) and specific state response (SS [47,48]). The LR approach considers that the solvent remains frozen during the electron transition. In this way the ground and excited states are perturbed by exactly the same solvent polarization. The SS method also fixes the orientational component but allows the electron degrees of freedom of the solvent, i.e., the electron or non-inertial polarization, to adjust in response to the change in the charge distribution of the solute during the transition. Three SS schemes were developed depending on whether the polarization of the solvent and the new electron density of the solute reached mutual equilibrium or not. Thus we have the corrected-Linear Response, cLR [49], the IBSF (Improta, Barone, Scalmani and Field) methods [50,51] and the Vertical Excitation Method (VEM) [52]. In this paper we used the PCM/cLR model as it combines a reliable performance with high computational efficiency. When a microscopic description of the solvent structure was needed, the ASEP/MD method was used. Both inertial and electron solvent polarizations are included in the current version [53].

Fig. 2 displays the basic scheme of ASEP/MD. This method introduces the Average Solvent Electrostatic Potential (ASEP) generated by the solvent as a perturbation into the Schrödinger equation. The ASEP is obtained from a molecular dynamic (MD) simulation in which the geometries and charges on the solute atoms are obtained from a quantum calculation of the solute molecule. As the charges, in turn, depend on the solvent perturbation, it was necessary to perform an iterative cycle. MD simulations were carried out using Gromacs [54–56] and included one 3–HF molecule surrounded by 397 ethanol molecules in a rhombic dodecahedral box. Lennard-Jones parameters for the solute and solvent were taken from all-atoms OPLS force field [57] and the atomic charges were calculated using the CHELPG method [58,59]. Periodic boundary conditions were applied in all directions. Short-range electrostatic interactions were cut-off at 1.3 nm and long-range interactions were calculated with the Particle-Mesh Ewald (PME) method [60]. The temperature was fixed at 300 K with the Nosé-Hoover thermostat [61]. Each simulation was run in the NVT ensemble for 1000 ps, with a time step of 1 fs, where the first 250 ps were used for equilibration and the last 750 ps for production. In solution results were obtained by averaging the last five ASEP/MD cycles, and therefore they represent a 3.75 ns average.

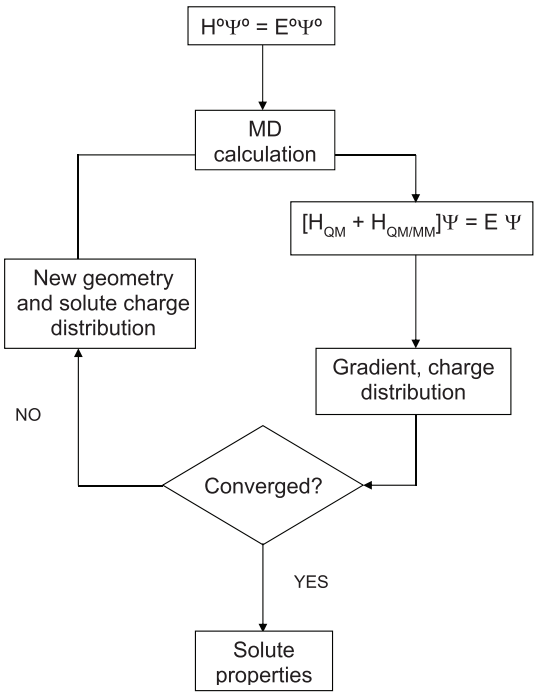

Fig. 2. ASEP/MD calculation scheme.

ASEP/MD geometry optimizations on the free energy surface [62] for both the ground and excited states were performed combining the free energy gradient method [63,64,65] and the mean field approximation [66,67]. Free energy differences between critical points on ground and excited state free energy surfaces were calculated using a dual-level methodology where the geometric and electronic polarization of the solute is quantum-mechanically described but where the solute–solvent interaction free energy is classically calculated through the free energy perturbation method [68,69]. In this approach, a perturbation parameter λ is introduced. When λ = 0, the solute geometry and atomic charges correspond to the initial state whereas when λ = 1 they correspond to the final state. These initial and final states are then connected by a linear interpolation using a value of Δλ = 0.005. Note that charges and geometries of the initial and final states are obtained from converged ASEP/MD calculations.

In our calculations we have also included the solvent electron polarization. Using the solvent structure and solute geometry obtained in the ASEP/MD self-consistent process, the quantum mechanical solute and the electron polarization of the solvent have been coupled. A molecular polarizability is assigned to every solvent molecule, and simultaneously, the effective solvent charge distribution used in the MD calculation is replaced by their gas phase values. The dipole moment induced on each solvent molecule is a function of the dipole moments induced on the rest of the molecules and of the solute charge distribution, and hence the electrostatic equation has to be solved self-consistently. The process finishes when convergence in the solute and solvent charge distribution is achieved. Details of the method can be found in Muñoz-Losa et al. [70].

Rate constants were computed at 300 K using Variational Transition State Theory (VTST) with a multiplicative semiclassical Multidimensional Tunneling (MT) correction [71,72]. In this approach

the rate constants, $k_{VTST/MT(T)}$, are calculated as the product of two factors:

$$k_{VTST/MT}(T) = \kappa_{tun}(T) \cdot k_{VTST}(T)$$

The first factor, $\kappa_{tun}(T)$, is the multidimensional tunneling correction. This factor is computed as the thermal-averaged tunneling probability of passing through a monodimensional barrier to reaction, which is computed in a multidimensional phase space. In this work we used the small-curvature approximation, which assumes that tunneling occurs within the vibrational valley, described by the minimum energy path and the vibrational turning points of the reactive system as it moves through this energy path. The most probable tunneling path connects the closest vibrational turning points in the reactant and product channels, so that the tunneling path is on the concave side of the reaction path. We assume that the curvature of the reaction path (measured as the coupling between the motion along the reaction path and vibrational motions) is small or moderate, and the system always remains in the vibrationally adiabatic ground state as it evolves from reactant to products. Because of the large number of vibrational modes and the low value of some of the vibrational frequencies, we assume that the tunneling energies used in our computations are a continuous function.

The second factor, $k_{VTST}(T)$ is the VTST semiclassical rate constant. In its canonical version used in this work, this rate constant is obtained by maximizing the free energy along the reaction path and using its maximum value to compute the rate constant by means of transition state theory. Bound vibrational modes are treated as quantum–mechanical harmonic oscillator, rotational partition functions were calculated classically, however, under the assumption that the vibrational modes are separable. Normal modes were computed using a system of redundant internal coordinates. All kinetics calculations were performed using the POLYRATE code [73], using as an input the geometries, energies and their first and second derivatives at stationary points and selected points on the reaction path obtained from Gaussian calculations in the excited state. Note that in these calculations we assume thermodynamical equilibrium as well as equilibrium solvation, i.e., that the solvent does not participate explicitly in the reaction coordinate.

2. Results and discussion

2.1. Gas phase

Table 1 displays the calculated vertical transition energies for the absorption ($S_0(N) \rightarrow S_1$ (FC)) and fluorescent emission (S_1-$(N^*) \rightarrow S_0(FC)^{N^*}$, ($S_1(T^*) \rightarrow S_0(FC)^{T^*}$) of 3–HF where FC, S_0 and S_1 refer to the Franck-Condon point, the ground state and the first excited state, respectively. Note that there is a single Franck-Condon structure in the absorption process, S_1 (FC), but the Franck-Condon S_0 points are different when emitting from $S_1(N^*)$, $S_0(FC)^{N^*}$, and from $S_1(T^*)$, $S_0(FC)^{T^*}$. TD-DFT results with three different functionals are shown. Both in absorption and in emission the orbitals involved are of π type (see Fig. 3) and these transitions can be described as π-π* [74]. The employed functional does not introduce significant differences in the orbital topology.

In gas phase, the B3LYP functional predicts an intense absorption band ($S_0(N) \rightarrow S_1(FC)$) placed at 3.56 eV. PBE0 and CAM-B3LYP give values of 3.68 and 4.02 eV, respectively. The experimental UV–Vis spectrum for 3–HF in non-polar solvents shows a very broad band with the maximum placed at 3.59 eV. The use of polar solvent does not produce significant changes in the position of this band, although in these solvents a new band of little intensity appears at 400 nm, that has been associated with the formation of the anionic form of 3–HF originated by the deprotonation of the 3-hydroxy group [14]. It is interesting to note that B3LYP and PBE0 results are in good agreement with the experimental value of 3.59 eV while CAM–B3LYP overestimates this transition.

Usually, the dipole moment variation during a transition plays an important role in the relative stabilization of the ground and excited states in solution and, consequently, in the calculation of the solvent shift. In gas phase, the $S_0(N) \rightarrow S_1(FC)$ vertical transition is accompanied by a slight increase of the dipole moment, 0.8 D (see Table 2), when calculated with B3LYP (from 3.41 D for the ground state to 4.24 D for the FC excited state). A similar but somewhat lower dipole moment increase was obtained with PBE0 and CAM-B3LYP functionals (0.6 D and 0.4 D, respectively). In all cases the direction of the dipole moment is nearly parallel to that of the carbonyl bond. Therefore, there are no appreciable changes during the electronic transition but there are changes in the transition from the N* form to the T* form, where the proton and hence the position of the carbonyl group are exchanged.

As for the emission $S_1(N^*) \rightarrow S_0(FC)^{N^*}$, transition appears at 3.14 eV (B3LYP), 3.23 eV (PBE0) and 3.47 eV (CAM-B3LYP). The emission from T* appears at lower energies: 2.29 eV, 2.40 eV and 2.47 eV with B3LYP, BPE0 and CAM-B3LYP, respectively. The Stokes shift is 0.42 eV for the emission from N* and 1.27 eV in the case of T*. Worthy of note is the important decrease in the value of the dipole moment when passing from the N* (4.23 D with B3LYP) to the T* form (2.40 D), which is expected to affect the relative stability of N* and T* in polar solvents.

Fig. 4 displays the energy diagram of 3–HF in gas phase (only the B3LYP results are shown). The potential energy profile along the reaction coordinate is also displayed. The adiabatic transitions to N* and T* excited states ($S_0(N) \rightarrow S_1(N^*)$ and $S_0(N) \rightarrow S_1(T^*)$) appear at 77.3 and 67.7 kcal/mol, respectively. Therefore, T* is 9.6 kcal/mol more stable that the N* form. The PBE0 functional provides very similar results whereas CAM-B3LYP increases the free energy of the ESIPT reaction to 11.0 kcal/mol. The gas-phase profile suggests a practically irreversible reaction shifted towards the T* species.

In gas phase, the proton transfer reaction must surmount a potential energy barrier of about 2.5 kcal/mol. The FC point is 4.8 kcal/mol above the N* minimum, so it can be concluded that the system has sufficient energy to easily surmount the barrier. Moreover, when entropic effects are included, the free energy barrier to reaction diminishes even further, to near 1 kcal/mol. The increase in the entropy of the transition state is due to the fact that the hydrogen being transferred is looser in the transition state than in the N form, since the O–H bond in the reactant is partially broken and the O–H bond in products is still not formed. The tunneling effect correction in gas phase was estimated to increase the rate constant by about 25%, further reducing the effective activation energy to only 0.6 kcal/mol. The estimated rate constant for the proton transfer reaction is shown in Table 3, and the computed N* half-life time is 0.44 ps (437 fs), a value lower than the experimental fluorescence time. In conclusion, the reaction is thermodynamically controlled, and the emission in gas phase is expected only to take place from the most stable form: the T* tautomer. It can be presumed that this will also be the case in non-polar solvents, as we will discuss below.

2.2. Ethanol solution

2.2.1. Absorption and emission spectra

In agreement with experimental findings, the calculated absorption transition energies in ethanol are similar to those found in gas phase (Table 1). PCM provides B3LYP and PBE0 values for the first electronic transition of 3.56 and 3.67 eV, respectively, these

Table 1
Electronic transition energies and solvent shifts, δ, of 3–HF in gas phase and in ethanol solution using different methods, in kcal/mol. In parentheses the transition energies in eV.

		B3LYP	PBE0	CAM-B3LYP	Exp.[a]
	Gas phase	82.12 (3.56)	84.87 (3.68)	92.71 (4.02)	
	PCM	82.13 (3.56)	84.64 (3.67)	92.71 (4.02)	
	δ	−0.02	−0.07	−0.15	
Absorption	**ASEP-MD**	81.64 (3.54)	84.64 (3.67)	92.02 (3.99)	82.79 (3.59)
	δ	−0.39	−0.05	−0.67	
	ASEP-MD^{pol}	81.41 (3.53)	84.64 (3.67)	92.02 (3.99)	
	δ	−0.76	−0.26	−0.83	
	Gas phase	72.41 (3.14)	74.49 (3.23)	80.03 (3.47)	
	PCM	71.03 (3.08)	73.11 (3.17)	77.49 (3.36)	
	δ	−1.25	−1.34	−2.41	
Emission (N)	**ASEP-MD**	71.72 (3.11)	74.03 (3.21)	78.64 (3.41)	70.57 (3.06)
	δ	−0.70	−0.58	−1.36	
	ASEP-MD^{pol}	71.49 (3.10)	73.34 (3.18)	78.41 (3.40)	
	δ	−0.86	−1.22	−1.59	
	Gas phase	52.71 (2.29)	55.35 (2.40)	56.96 (2.47)	
	PCM	54.43 (2.36)	56.27 (2.44)	57.66 (2.50)	
	δ	1.64	1.08	0.82	
Emission (T)	**ASEP-MD**	53.27 (2.31)	55.35 (2.40)	57.66 (2.50)	53.97 (2.34)
	δ	0.51	0.00	0.86	
	ASEP-MD^{pol}	53.5 (2.32)	55.58 (2.41)	58.12 (2.52)	
	δ	0.78	0.22	1.19	

*Includes the contribution of the electron solvent polarization.
[a]Experimental values in ethanol solution from Ref. 24.

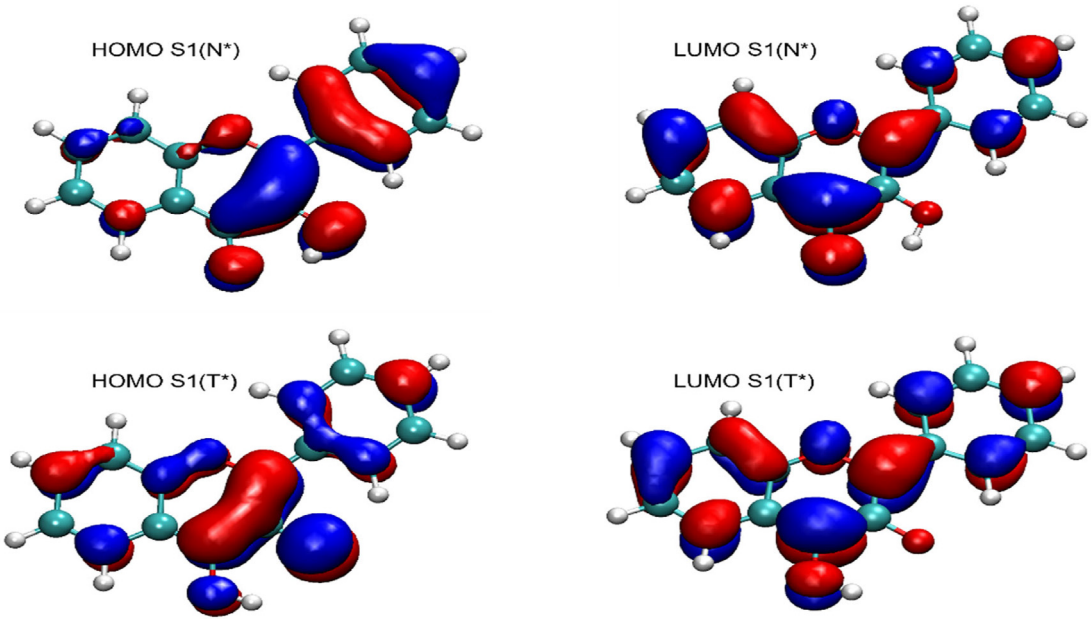

Fig. 3. HOMO and LUMO orbitals for the $S_1(N^*) \rightarrow S_0(FC)$ and $S_1(T^*) \rightarrow S_0(FC)$ transitions. Orbitals involved in the $S_0(N) \rightarrow S_1(FC)$ absorption are similar. In all the transitions the calculated oscillator strength has a value of around 0.4.

values being in good agreement with the experimental data and with the results found in the literature. CAM-B3LYP again overestimates the transition energy in 0.40 eV. This poor performance of CAM-B3LYP will also be observed in the emission spectrum. The ASEP/MD method yields 3.53 (B3LYP), 3.67 (PBEO) and 3.99 eV (CAM-B3LYP), regardless of whether electron solvent polarization is considered (ASEP/MD^{pol}) or not (ASEP/MD). Thus, both the PCM and the ASEP/MD methods provide similar results.

Regarding the solvent shift it can be observed that its value for the absorption transition energy is very small, −0.02 kcal/mol with PCM and −0.76 kcal/mol with ASEP/MD (B3LYP values). In order to understand the limited influence of the solvent on absorption it is interesting to analyze the change in the solute charge distribution during the transition and the effect of the solvent (see Table 2). As expected, the solvent polarizes the solute increasing the dipole moment of the different states, and this increase is larger with ASEP/MD than with PCM. However, the change in the dipole moment during the transition, which determines the size of the solvent shift, decreases in solution. So, the dipole variation during the vertical excitation decreases from 0.8 D in gas phase to only 0.4 D and 0.3 D in ethanol solution with PCM and ASEP/MD^{pol}, respectively (B3LYP values).

With regard to the emission from N*, solvent effects are not noticeable either. In gas phase this emission is placed between

Table 2
Dipole moments values (Debye) for the different species in gas phase and in ethanol solution.

Absorption							
		S_0			FC		
		B3LYP	PBE0	CAM-B3LYP	B3LYP	PBE0	CAM-B3LYP
N	**Gas Phase**	3.41	3.38	3.39	4.24	4.04	3.77
	PCM	5.07	4.86	4.88	5.47	5.21	5.17
	ASEP/MD	5.39	5.10	5.36	5.49	5.10	5.50
	ASEP/MD^{pol}	5.61	5.29	5.55	5.94	5.37	5.78
T	**Gas Phase**	4.42	4.46	4.84	2.38	2.39	2.65
	PCM	6.60	6.56	7.07	3.80	3.74	4.12
Emission							
		S_1			FC		
		B3LYP	PBE0	CAM-B3LYP	B3LYP	PBE0	CAM-B3LYP
N*	**Gas Phase**	4.23	3.96	3.73	3.69	3.72	3.81
	PCM	5.52	5.26	5.41	5.12	5.05	4.88
	ASEP/MD	6.97	6.87	6.81	5.20	5.42	6.11
	ASEP/MD^{pol}	7.28	7.08	7.15	5.61	5.63	6.46
T*	**Gas Phase**	2.40	2.36	2.59	4.35	4.30	4.57
	PCM	3.44	3.60	3.88	5.52	5.47	5.82
	ASEP/MD	3.11	2.94	3.40	4.86	4.55	5.28
	ASEP/MD^{pol}	3.20	3.03	3.49	5.04	4.83	5.42

*Includes the contribution of the electron solvent polarization.

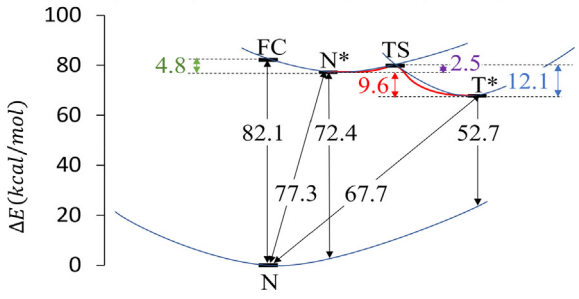

Fig. 4. Potential energy diagram of 3–HF in gas phase. The horizontal axis represents an imaginary collective reaction coordinate.

3.14 and 3.47 eV, depending on the functional used. The B3LYP/PCM method provides a transition energy in ethanol solution of 3.08 eV, in good agreement with the experiment (3.06 eV), and a red solvent shift of about −1.2 kcal/mol. Very similar results (3.10 eV for the transition energy and 0.86 kcal/mol for the solvent shift) are obtained with B3LYP/ASEP/MD^{pol}. This result is striking since in this case the in-solution dipole variations can be important depending on the solvent description, PCM or ASEP/MD. Thus, although with B3LYP/PCM the variation is only 0.4 D (the dipole goes from 5.52 in S1 to 5.12 D in S0), with ASEP/MD the dipole varies by about 1.7 D. However, these differences in the magnitude of the dipole moments do not translate to differences in the solvent shift. It can be concluded that for this system, the dipole moment variation does not seem to be a good predictor of the solvent shift, and that higher order multipole moments could play an important role.

In contrast to the red shift found in ethanol solution for absorption from N and fluorescence from N*, emission from T* displays a slightly blue solvent shift. The experiments place this band at 2.34 eV, in very good agreement with the PCM (2.36 eV, B3LYP) and ASEP/MD (2.32 eV, B3LYP/ASEP/MD^{pol}) results. The blue solvent shifts are 1.64 kcal/mol (PCM) and 0.78 kcal/mol (ASEP/MD^{pol}).

Once the main characteristics of the 3–HF spectra are known, the shift of the emission bands with respect to the absorption band, known as Stokes shift, can be calculated. Independently of the solvent model used, a Stokes shift of 0.48 and 1.20 eV was obtained for transitions from N* and T* forms, respectively. These values are similar to those found in gas phase (0.42 and 1.27 eV) and they confirm the trend found in absorption: the solvent hardly affects the position of the bands.

Next, we will analyze the changes in the solvent structure during the excitation and subsequent ESIPT reaction, i.e., during the relaxation from the FC to the N* minimum and from there to the T* minimum. Figs. 5 and 6 show the pair radial distribution functions (RDF) of the atoms involved in the proton transfer reaction. In the ground state a strong hydrogen bond O_4-H_a is formed between the 3–HF carboxylic oxygen and the alcoholic hydrogen of an ethanol molecule (H_a), with a coordination number of 0.94. In contrast, O_3 does not form intermolecular hydrogen bond. During the relaxation from the FC point to the N* minimum, the height of the first peak of the O_4-H_a RDF increases, with a coordination number of 1.15. As with the situation in the ground state, O_3 remains without an important hydrogen bond interaction with the solvent. H_3 seems to produce a more structured solvent as the first peak of the RDF corresponding to the distances between H_3 and the alcoholic oxygen, O_a, appears more defined, with coordination numbers from 0.33 at N to 0.51 at N*. During the ESIPT reaction H_3 is transferred from O_3 to O_4, which is reflected in the loss of the solvent structure around O_4, now part of the hydroxyl group (Fig. 6). It is worth noting that the intramolecular hydrogen bond seems to be weaker than in N* given the presence of a more structured solvent around H_3, the coordination numbers at T* rise to 0.71 in the H3-Oa and to 0.44 in the O3-Ha.

Table 3
Barrier heights, rate constants without (k_{VTST}) and with ($k_{VTST/MT}$) tunneling corrections, tunneling corrections and Arrhenius activation energies without (E_a^{TS}) and with (E_a^{MT}) tunneling corrections of the ESIPT reaction of 3–HF from N* to T* form. Half-life time of 3–HF. Results are computed in gas phase and in ethanol and cyclohexane (PCM).

	ΔE^{TS}(kcal/mol)	k_{VTST} (s^{-1})	κ_{tun}	$k_{VTST/MT}$ (s^{-1})	E_a^{TS} (kcal/mol)	E_a^{MT} (kcal/mol)	$t_{½}$(ps)
Gas phase	2.57	$1.3{\cdot}10^{12}$	1.25	$1.6{\cdot}10^{12}$	0.78	0.55	0.43
Cyclohexane	2.84	$8.2{\cdot}10^{11}$	1.36	$1.1{\cdot}10^{12}$	0.99	0.57	0.58
Ethanol	3.52	$3.3{\cdot}10^{11}$	1.75	$5.8{\cdot}10^{11}$	1.57	0.97	1.18

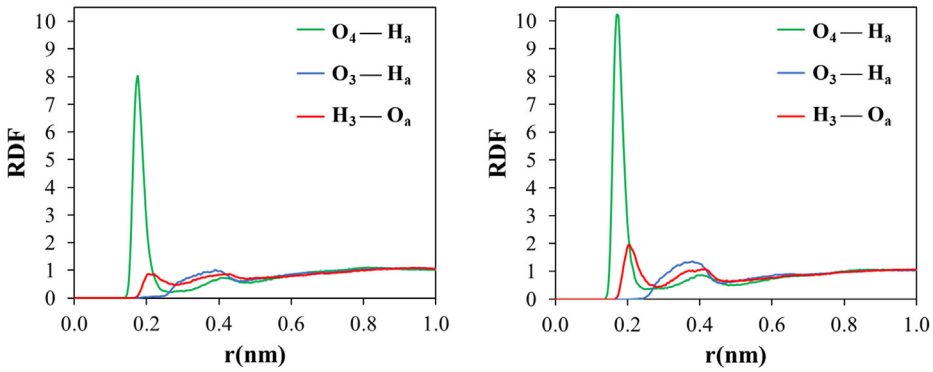

Fig. 5. Radial distribution functions for the ground state (N, left panel) and excited state (N*, right panel) of 3–HF normal form in ethanol. Red line: RDFs of the distance between H_3 and alcoholic oxygen; blue line: RDFs of the distance between O_3 and alcoholic hydrogen; green line: RDFs of the distance between O_4 and alcoholic hydrogen. (For interpretation of the references to color in this figure legend, the reader is referred to the web version of this article.)

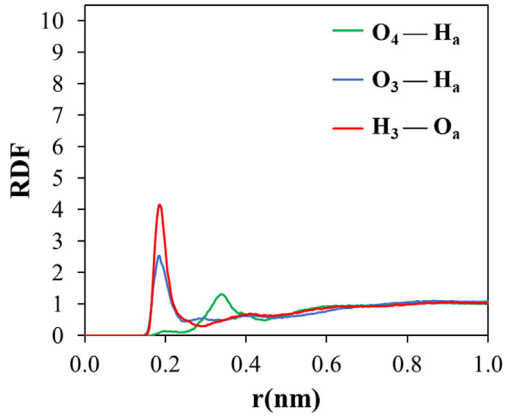

Fig. 6. Radial distribution functions for the excited state of 3–HF tautomeric form in ethanol. The color line code is the same as in Fig. 5.

In sum, effects of the solvent on the band position are in general small, although in some cases the variations of the dipole moment during the transition can be large. There are no appreciable differences between the values of the transition energies provided by PCM and ASEP/MD and, in the latter method, between polarizable and non-polarizable solvent. This behavior is likely the results of two factors: on the one hand, the solvent shift in this system is very small and, in consequence, it is difficult to distinguish the contributions of bulk solvent and specific interactions; on the other hand, so far we have only considered vertical transitions, situations in which the solvent structure is the same in the initial and final state, and which can favor the error compensation.

2.2.2. Description of the free energy surface in the excited state

Table 4 and Fig. 7 display the free energy profile of the excited state proton transfer reaction calculated with both PCM and ASEP/MD methods. All energies refer to the energy of the minimum of the normal form in the ground state. Although the general appearance of the surface is the same with the two methods (similar position of the FC absorption state, T* minimum more stable than N* minimum), the relative stability of the various points differs from PCM to ASEP/MD. Thus, the adiabatic transition from S_0, N → N*, is placed at 77.2 kcal/mol with PCM but at 80.5 kcal/mol with ASEP/MD. However, the two methods place the T* state at almost the same energy, 68.8 kcal/mol with PCM and 68.7 kcal/mol with ASEP/MD. The T* state is more stable than the N* state by about 8.4 kcal/mol when PCM is used and 11.8 kcal/mol when specific interactions (ASEP/MD) are included. From a thermodynamic point of view, the emission from the tautomeric form is clearly favored.

Some authors have proposed that in solvents that form hydrogen bonds the loss or reduction of the T* emission signal is due to the stabilization of an alternate form that does not form an intramolecular hydrogen bond in the ground state (A form) [22]. This conformer has an absorption and fluorescence spectrum completely equivalent to N. However, no theoretical study has addressed this issue, to the best of our knowledge. Therefore, in order to test the validity of this hypothesis we analyzed the relative stability of the two conformers, N and A. Both PCM and ASEP/MD yield a free energy difference about 5–6 kcal/mol in ethanol solution, the conformational equilibrium being clearly shifted towards the normal conformer. To better describe the specific interaction with solvent molecules, we also performed calculations explicitly including one or two ethanol molecules. These studies show that the energy difference between the two conformers reduces up to 2.0–2.5 kcal/mol. Thus, in any case, independently of the solvent model employed, the normal form is clearly favored and the population of the A conformer at room temperature is always lower than 3.5%. In sum, the presence of the A conformer and the conformational equilibrium between A and N* could account only for a small reduction of the T* emission band (as it slightly decreases the concentration of the reactive form N*) but it can never explain the strong reduction of the signal in the proton donor–acceptor solvents.

Next, the kinetics of the ESIPT reaction in solution was calculated. The results are shown in Table 3. First we describe the results provided by the PCM method. To analyze the effect of the polarity of the solvent, we also perform kinetics calculations on cyclohexane solution. The height of the barrier in cyclohexane is 2.84 kcal/mol, very similar to the gas-phase barrier height, 2.57 kcal/mol. The entropic effects discussed above lower this barrier to 0.99 kcal/mol, only slightly higher than the gas phase value, 0.78 kcal/mol. As for polar solvents, Salaeh et al. [8] studied the effect of including a specific methanol molecule on the barrier height, finding a value of 2.88 kcal/mol. However, our calculations show that in ethanol the barrier height increases significantly, up to 3.52 kcal/mol, 1.57 kcal/mol upon inclusion of entropic effects, which is about twice the gas-phase barrier height. However, since the absorption FC point is 4.90 kcal/mol about the N* minimum, in principle, the system has enough energy to surmount the barrier.

So far we have considered only the thermal overcoming of the barrier; for a detailed description of the process, we now need to consider tunneling. The model we use again is that developed by Truhlar and coworkers [71,72]. The results are displayed in Table 3. In gas phase and cyclohexane the half-life times are very similar,

Table 4
Free energy transition between N, N* and T* states (kcal/mol) in gas phase and in ethanol solution.

	Gas phase			PCM			ASEP-MD		
	B3LYP	PBE0	CAM-B3LYP	B3LYP	PBE0	CAM-B3LYP	B3LYP	PBE0	CAM-B3LYP
N – N*	77.30	79.71	86.35	77.25	79.57	85.84	80.51	83.26	94.75
N – T*	67.74	70.29	75.34	68.84	71.16	76.18	68.74	70.99	75.89
N* – T*	9.56	9.41	11.01	8.41	8.41	9.66	11.77	12.27	18.86

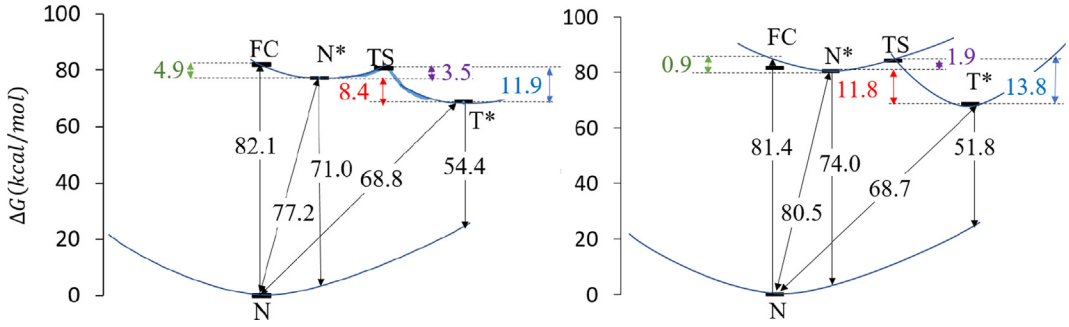

Fig. 7. Energy diagram of 3–HF in ethanol solution computed using PCM (left panel) and ASEP/MD (right panel) methods. The horizontal axis represents an imaginary collective reaction coordinate.

but there is an important reduction when passing to ethanol solution. Even though in this case tunneling becomes more important (it increases the rate constant by roughly a factor of 2), due to the higher barrier the reaction is still slower than in gas phase. The effective activation energy for the proton transfer computed including tunneling is 0.97 kcal/mol, making the half-life time of N*, 1193 fs, larger than the fluorescent half-life. Therefore, the emission from N* is possible, explaining the loss of the fluorescent signal, which does not occur in gas phase or cyclohexane solution. It must be noted, however, that the calculation of this tunneling factor also assumes equilibrium solvation, which is a somewhat crude approximation since tunneling is a non-equilibrium situation. Thus, tunneling probabilities are likely to diminish even further in ethanol solution, since this solvent is expected to be more strongly coupled to the solute.

Finally, in order to determine the effect of specific interactions, the proton transfer barrier height in ethanol was calculated with ASEP/MD using the geometry of the transition state obtained with PCM, i.e., the geometries were not re-optimized, only the free energy differences between the critical points of the reaction were recalculated. It is important to note that these values were obtained assuming equilibrium solvation. This regime is valid in a non-polar solvent such as cyclohexane, but it provides only approximate values in a polar solvent such as ethanol, where non-equilibrium solvation could modify the barrier height. The barrier height is somewhat lower than that found with PCM (1.95 *vs* 3.52 kcal/mol). However, as ASEP/MD destabilizes the N* form with respect to the ground state, so that the transition state is now above the FC point, decreasing the probability of overcoming the barrier. We must again stress that these free energy differences were calculated using an equilibrium solvent model. In polar environment the time scale of the solvent response varies between a few ps (inertial response) to several ps or ns (rotational and translational diffusive response). The half-life time of the proton transfer reaction is 0.6 ps in cyclohexane and 1.19 in ethanol, being the barrier passage times even lower. In these conditions, it can be expected that solvent and reaction coordinates are tightly entangled. The consideration of a non-equilibrium solvent would likely increase the barrier height, decreasing even more the probability of transition. As a consequence, the probability that the system surmounts the barrier can decrease notably and explain the loss of the emission signal from T* in the ethanol solution.

3. Conclusions

In this work, the photophysics and photochemistry of 3–HF were studied in solution using PCM and ASEP/MD methods. The comparison of the results provided by the two methods permits us to determine the role played by bulk and specific interactions.

It was found that both in absorption and emission the orbitals involved are of π type and these transitions can be described as π-π*. In gas phase an intense absorption band is predicted, and the vertical transition slightly reduces the dipole moment. The emission $S_1(N^*) \rightarrow S_0(FC)$ appears at higher energies than the emission from T*, the latter showing a significantly lower dipole moment and higher stability, so that the N* to T* equilibrium is shifted towards the T* species and the proton transfer has a potential energy barrier of about 2.5 kcal/mol, although the phenomenological activation energy is only 0.6 kcal/mol. Since the FC point is 4.8 kcal/mol above the N* minimum, the system has sufficient energy to easily surmount the barrier. Therefore, only T* emission is predicted in the gas phase. The same conclusion is obtained from calculations in a non-polar solvent, cyclohexane.

Polar solvents (ethanol) hardly modify the absorption and emission bands. A new absorption band appears at 400 nm because of the deprotonation of the 3-hydroxy group [14], and the emission from N* shows a small red shift, while the emission from T* is slightly blue-shifted. Although charge fluxes are more noticeable than in gas phase, the charge separation diminishes, and the proton transfer reaction is favored.

However, ethanol solvent has a significant impact on the kinetics of the proton transfer reaction, from N* to T*. The T* state is more stable than the N* state by about 8.4 kcal/mol when PCM is used, increasing to 11.8 kcal/mol when specific interactions (ASEP/MD) are included, and the barrier height increases significantly with respect to gas-phase, up to 3.52 kcal/mol, with a phenomenological activation energy or roughly 1 kcal/mol, which is about twice the activation energy computed in the gas phase. Thus, in this solvent the half-life time is larger than the fluorescent half-

life, making the emission from N* possible and the loss of signal from T* emission.

Finally, to rule out the presence of the A form as the cause of the loss of signal, we estimated the population of the A conformer. We found that an upper estimation of A population is 3.5% with respect to N*. Therefore, our main conclusion from the present study is that the loss of the emission signal from T* is due to the slower proton transfer reaction in ethanol solution with respect to gas phase or non-polar solvents.

Author Contributions

All the authors equally contributed to software development, computations, formal analysis, investigation, visualization and writing of the original draft. J.C.C., M.E.M. and M.L.S. were responsible for funding administration.

Data availability

Data will be made available on request.

Declaration of Competing Interest

The authors declare that they have no known competing financial interests or personal relationships that could have appeared to influence the work reported in this paper.

Acknowledgements

This work is partially supported by Junta de Extremadura and European Regional Development Fund, Spain (Projects GR21032, GR21036 and IB18022). S.F.P. and M.J.C. thank Junta de Extremadura for their research contracts associated with the IB18022 grant.

References

[1] S. Quideau, Flavonoids. Chemistry, biochemistry and applications. Edited by Øyvind M. Andersen and Kenneth R. Markham., Angew. Chemie Int. Ed. 45(41) (2006), doi: 10.1002/anie.200685399.
[2] P.K. Sengupta, M. Kasha, Excited state proton-transfer spectroscopy of 3-hytdroxyflavone and quercetin, Chem. Phys. Lett. 68 (2–3) (1979) 382–385, https://doi.org/10.1016/0009-2614(79)87221-8.
[3] S. Protti, A. Mezzetti, Any colour you like. Excited state and ground state proton transfer in flavonols and applications, Photochemistry 40 (2012) 295–322, https://doi.org/10.1039/9781849734882-00295.
[4] A.S. Klymchenko, V.G. Pivovarenko, T. Ozturk, A.P. Demchenko, Modulation of the solvent-dependent dual emission in 3-hydroxychromones by substituents, New J. Chem. 27 (9) (2003) 1336–1343, https://doi.org/10.1039/b302965d.
[5] D. Loco, S. Protti, B. Mennucci, A. Mezzetti, Critical assessment of solvent effects on absorption and fluorescence of 3HF in acetonitrile in the QM/PCM framework: a synergic computational and experimental study, J. Mol. Struct. 1182 (2019) 283–291, https://doi.org/10.1016/j.molstruc.2018.12.085.
[6] P.K. Sengupta, Pharmacologically active plant flavonols as proton transfer based multiparametric fluorescence probes targeting biomolecules: perspectives and prospects, 2017, pp. 45–70.
[7] S. Höfener, P.C. Kooijman, J. Groen, F. Ariese, L. Visscher, Fluorescence behavior of (selected) flavonols: a combined experimental and computational study, PCCP 15 (30) (2013) 12572–12581, https://doi.org/10.1039/c3cp44267e.
[8] R. Salaeh, C. Prommin, W. Chansen, K. Kerdpol, R. Daengngern, N. Kungwan, The effect of protic solvents on the excited state proton transfer of 3-hydroxyflavone: a TD-DFT static and molecular dynamics study, J. Mol. Liq. 252 (2018) 428–438, https://doi.org/10.1016/j.molliq.2017.12.148.
[9] S. Protti, A. Mezzetti, Solvent effects on the photophysics and photoreactivity of 3-hydroxyflavone: a combined spectroscopic and kinetic study, J. Mol. Liq. 205 (2015) 110–114, https://doi.org/10.1016/j.molliq.2014.12.001.
[10] D. McMorrow, M. Kasha, Intramolecular excited-state proton transfer in 3-hydroxyflavone. Hydrogen-bonding solvent perturbations, J. Phys. Chem. 88 (11) (1984) 2235–2243, https://doi.org/10.1021/j150655a012.
[11] A.J.G. Strandjord, P.F. Barbara, Proton-transfer kinetics of 3-hydroxyflavone: solvent effects, J. Phys. Chem. 89 (11) (1985) 2355–2361, https://doi.org/10.1021/j100257a041.
[12] G.A. Brucker, T.C. Swinney, D.F. Kelley, Proton-transfer and solvent polarization dynamics in 3-hydroxyflavone, J. Phys. Chem. 95 (8) (1991) 3190–3195, https://doi.org/10.1021/j100161a043.
[13] A.N. Bader, F. Ariese, C. Gooijer, Proton transfer in 3-hydroxyflavone studied by high-resolution 10 K laser-excited Shpol'skii spectroscopy, Chem. A Eur. J. 106 (12) (2002) 2844–2849, https://doi.org/10.1021/jp013840o.
[14] S. Lazzaroni, D. Dondi, A. Mezzetti, S. Protti, Role of solute-solvent hydrogen bonds on the ground state and the excited state proton transfer in 3-hydroxyflavone. A systematic spectrophotometric study, Photochem. Photobiol. Sci. 17 (7) (2018) 923–933, https://doi.org/10.1039/c8 pp00053k.
[15] P. Zhou, K. Han, Unraveling the detailed mechanism of excited-state proton transfer, Acc. Chem. Res. 51 (7) (2018) 1681–1690, https://doi.org/10.1021/acs.accounts.8b00172.
[16] C.C. Hsieh, C.M. Jiang, P.T. Chou, Recent experimental advances on excited-state intramolecular proton coupled electron transfer reaction, Acc. Chem. Res. 43 (10) (2010) 1364–1374, https://doi.org/10.1021/ar1000499.
[17] F.S. Santos, E. Ramasamy, V. Ramamurthy, F.S. Rodembusch, Excited state chemistry of flavone derivatives in a confined medium: ESIPT emission in aqueous media, Photochem. Photobiol. Sci. 13 (7) (2014) 992–996, https://doi.org/10.1039/c4 pp00096j.
[18] A.C. Sedgwick et al., Excited-state intramolecular proton-transfer (ESIPT) based fluorescence sensors and imaging agents, Chem. Soc. Rev. 47 (23) (2018) 8842–8880, https://doi.org/10.1039/c8cs00185e.
[19] S. Protti, K. Raulin, O. Cristini, C. Kinowski, S. Turrell, A. Mezzetti, Wavelength shifting systems based on flavonols and their metal complexes encapsulated by post-doping in porous SiO2 xerogel matrices, J. Mol. Struct. 993 (1–3) (2011) 485–490, https://doi.org/10.1016/j.molstruc.2011.02.010.
[20] F.J. Aparicio et al., Dye-based photonic sensing systems, Sensors Actuators, B Chem. 228 (2016) 649–657, https://doi.org/10.1016/j.snb.2016.01.092.
[21] E. Karakuş, M. Üçüncü, M. Emrullahoğlu, Electrophilic cyanate as a recognition motif for reactive sulfur species: selective fluorescence detection of H2S, Anal. Chem. 88 (1) (2016) 1039–1043, https://doi.org/10.1021/acs.analchem.5b04163.
[22] V.I. Tomin, A.P. Demchenko, P.T. Chou, Thermodynamic vs. kinetic control of excited-state proton transfer reactions, J Photochem Photobiol C: Photochem Rev 22 (2015) 1–18, https://doi.org/10.1016/j.jphotochemrev.2014.09.005.
[23] A.N. Bader, V. Pivovarenko, A.P. Demchenko, F. Ariese, C. Gooijer, Solvent influence on excited-state intramolecular proton transfer in 3-hydroxychromone derivatives studied by cryogenic high-resolution fluorescence spectroscopy, Spectrochim. Acta - Part A Mol. Biomol. Spectrosc. 59 (7) (2003) 1593–1603, https://doi.org/10.1016/S1386-1425(02)00361-X.
[24] S. Ameer-Beg et al., Ultrafast measurements of excited state intramolecular proton transfer (ESIPT) in room temperature solutions of 3-hydroxyflavone and derivatives, Chem. A Eur. J. 105 (15) (2001) 3709–3718, https://doi.org/10.1021/jp0031101.
[25] K. Chevalier, M.M.N. Wolf, A. Funk, M. Andres, M. Gerhards, R. Diller, Transient IR spectroscopy and ab initio calculations on ESIPT in 3-hydroxyflavone solvated in acetonitrile, PCCP 14 (43) (2012) 15007–15020, https://doi.org/10.1039/c2cp41077j.
[26] S. Chibani, Š. Budzák, M. Medved', B. Mennucci, D. Jacquemin, Full cLR-PCM calculations of the solvatochromic effects on emission energies, Phys. Chem. Chem. Phys. 16(47) (2014) 26024–26029, doi: 10.1039/c4cp03919j.
[27] R. Casadesús, O. Vendrell, M. Moreno, J.M. Lluch, K. Morokuma, On the intramolecular proton transfer of 3-hydroxyflavone in the first singlet excited state: a theoretical study, Chem. Phys. 325 (2–3) (2006) 243–250, https://doi.org/10.1016/j.chemphys.2005.12.028.
[28] C. Sukpattanacharoen, R. Salaeh, V. Promarak, D. Escudero, N. Kungwan, Heteroatom substitution effect on electronic structures, photophysical properties, and excited-state intramolecular proton transfer processes of 3-hydroxyflavone and its analogues: a TD-DFT study, J. Mol. Struct. 1195 (2019) 280–292, https://doi.org/10.1016/j.molstruc.2019.05.113.
[29] C. Lee, W. Yang, R.G. Parr, Development of the Colle-Salvetti correlation-energy formula into a functional of the electron density, Phys. Rev. B 37 (2) (1988) pp, https://doi.org/10.1103/PhysRevB.37.785.
[30] C. Adamo, V. Barone, Toward reliable density functional methods without adjustable parameters: the PBE0 model, J. Chem. Phys. 110 (13) (1999) 6158, https://doi.org/10.1063/1.478522.
[31] T. Yanai, D.P. Tew, N.C. Handy, A new hybrid exchange-correlation functional using the Coulomb-attenuating method (CAM-B3LYP), Chem. Phys. Lett. 393 (1–3) (2004) 51–57, https://doi.org/10.1016/j.cplett.2004.06.011.
[32] Y. Jiang, Y. Peng, Excited-state intramolecular proton transfer reaction of 3-hydroxyflavone, J. Clust. Sci. 26 (6) (2015) 1983–1992, https://doi.org/10.1007/s10876-015-0893-7.
[33] S. Takeuchi, T. Tahara, Coherent nuclear wavepacket motions in ultrafast excited-state intramolecular proton transfer: Sub-30-fs resolved pump-probe absorption spectroscopy of 10-hydroxybenzo[h]quinoline in solution, Chem. A Eur. J. 109 (45) (2005) 10199–10207, https://doi.org/10.1021/jp0519013.
[34] Y. Yang, Y. Liu, D. Yang, H. Li, K. Jiang, J. Sun, Photoinduced excited state intramolecular proton transfer and spectral behaviors of Aloesaponarin 1, Spectrochim. Acta - Part A Mol Biomol. Spectrosc. 151 (2015) 814–820, https://doi.org/10.1016/j.saa.2015.07.046.
[35] C. Prommin et al., Theoretical Insights on Solvent Control of Intramolecular and Intermolecular Proton Transfer of 2-(2′-Hydroxyphenyl)benzimidazole, Chem. A Eur. J. 121 (31) (2017) 5773–5784, https://doi.org/10.1021/acs.jpca.7b03454.

[36] W. Chansen, R. Salaeh, C. Prommin, K. Kerdpol, R. Daengngern, N. Kungwan, Theoretical study on influence of geometry controlling over the excited-state intramolecular proton transfer of 10-hydroxybenzo[h]quinoline and its derivatives, Comput. Theor. Chem. 1113 (2017) 42–51, https://doi.org/10.1016/j.comptc.2017.05.008.
[37] M.J. Frisch et al., Gaussian16 (Revision A.03), Gaussian Inc. Wallingford CT, Gaussian16 (Revision A.03). 2016.
[38] J. Tomasi, B. Mennucci, R. Cammi, Quantum mechanical continuum solvation models, Chem. Rev. 105 (8) (2005) 2999–3094, https://doi.org/10.1021/cr9904009.
[39] B. Mennucci, E. Cancès, J. Tomasi, Evaluation of solvent effects in isotropic and anisotropic dielectrics and in ionic solutions with a unified integral equation method: theoretical bases, computational implementation, and numerical applications, J. Phys. Chem. B 101 (49) (1997) 10506–10517, https://doi.org/10.1021/jp971959k.
[40] E. Cancès, B. Mennucci, J. Tomasi, A new integral equation formalism for the polarizable continuum model: theoretical background and applications to Isotropic and anisotropic dielectrics, J. Chem. Phys. 107 (8) (1997) 3032–3041, https://doi.org/10.1063/1.474659.
[41] M.L. Sanchez, M.A. Aguilar, F.J. Olivares Del Valle, Study of solvent effects by means of averaged solvent electrostatic potentials obtained from molecular dynamics data, J. Comput. Chem. 18(3) (1997), doi: 10.1002/(SICI)1096-987X(199702)18:3<313::AID-JCC2>3.0.CO;2-X.
[42] I.F. Galván, M.L. Sánchez, M.E. Martín, F.J. Olivares del Valle, M.A. Aguilar, ASEP/MD: A program for the calculation of solvent effects combining QM/MM methods and the mean field approximation, Comput. Phys. Commun. 155 (3) (2003) 244–259, https://doi.org/10.1016/S0010-4655(03)00351-5.
[43] D. Loco, N. Gelfand, S. Jurinovich, S. Protti, A. Mezzetti, B. Mennucci, Polarizable QM/Classical approaches for the modeling of solvation effects on UV-Vis and fluorescence spectra: an integrated strategy, Chem. A Eur. J. 122 (1) (2018) 390–397, https://doi.org/10.1021/acs.jpca.7b10463.
[44] M.E. Martín et al., Theoretical study of the role of solvent Stark effect in electron transitions, Theor. Chem. Acc. 128 (4) (2011) 783–793, https://doi.org/10.1007/s00214-010-0839-y.
[45] R. Cammi, B. Mennucci, Linear response theory for the polarizable continuum model, J. Chem. Phys. 110 (20) (1999) 9877–9886, https://doi.org/10.1063/1.478861.
[46] M. Cossi, V. Barone, Time-dependent density functional theory for molecules in liquid solutions, J. Chem. Phys. 115 (10) (2001) 4708–4717, https://doi.org/10.1063/1.1394921.
[47] C.A. Guido, G. Scalmani, B. Mennucci, D. Jacquemin, Excited state gradients for a state-specific continuum solvation approach: the vertical excitation model within a Lagrangian TDDFT formulation, J. Chem. Phys. 146(20) (2017) 204106-1-204106–9, doi: 10.1063/1.4983696.
[48] J.M. Mewes, J.M. Herbert, A. Dreuw, On the accuracy of the general, state-specific polarizable-continuum model for the description of correlated ground- and excited states in solution, PCCP 19 (2) (2017) 1644–1654, https://doi.org/10.1039/c6cp05986d.
[49] M. Caricato *et al.*, Formation and relaxation of excited states in solution: A new time dependent polarizable continuum model based on time dependent density functional theory, J. Chem. Phys. 124(12) (2006) 124520-1-124520–13, doi: 10.1063/1.2183309.
[50] R. Improta, V. Barone, G. Scalmani, M.J. Frisch, A state-specific polarizable continuum model time dependent density functional theory method for excited state calculations in solution, J. Chem. Phys. 125(5) (2006) 074504-1-074504–9, doi: 10.1063/1.2222364.
[51] R. Improta, G. Scalmani, M.J. Frisch, V. Barone, Toward effective and reliable fluorescence energies in solution by a new state specific polarizable continuum model time dependent density functional theory approach, J. Chem. Phys. 127(7) (2007) 074504-1-074504–9, doi: 10.1063/1.2757168.
[52] A.V. Marenich et al., Practical computation of electronic excitation in solution: vertical excitation model, Chem. Sci. 2 (11) (Oct. 2011) 2143–2161, https://doi.org/10.1039/C1SC00313E.
[53] F.F. García-Prieto, I.F. Galván, A. Muñoz-Losa, M.A. Aguilar, M.E. Martín, Solvent effects on the absorption spectra of the para-coumaric acid chromophore in its different protonation forms, J. Chem. Theory Comput. 9 (10) (2013) pp, https://doi.org/10.1021/ct400145z.
[54] Lindahl, Abraham, Hess, and van der Spoel, "GROMACS 2021.2 Source code," May 2021, doi: 10.5281/ZENODO.4723562.
[55] H.J.C. Berendsen, D. van der Spoel, R. van Drunen, GROMACS: A message-passing parallel molecular dynamics implementation, Comput. Phys. Commun. 91 (1–3) (Sep. 1995) 43–56, https://doi.org/10.1016/0010-4655(95)00042-E.
[56] S. Pronk et al., GROMACS 4.5: a high-throughput and highly parallel open source molecular simulation toolkit, Bioinformatics 29 (7) (Apr. 2013) 845–854, https://doi.org/10.1093/BIOINFORMATICS/BTT055.
[57] W.L. Jorgensen, D.S. Maxwell, J. Tirado-Rives, Development and testing of the OPLS all-atom force field on conformational energetics and properties of organic liquids, J. Am. Chem. Soc. 118 (45) (1996) 11225–11236, https://doi.org/10.1021/JA9621760.
[58] L.E. Chirlian, M.M. Francl, Atomic charges derived from electrostatic potentials: a detailed study, J. Comput. Chem. 8 (6) (1987) 894–905, https://doi.org/10.1002/JCC.540080616.
[59] C.M. Breneman, K.B. Wiberg, Determining atom-centered monopoles from molecular electrostatic potentials. The need for high sampling density in formamide conformational analysis, J. Comput. Chem. 11 (3) (1990) 361–373, https://doi.org/10.1002/JCC.540110311.
[60] T. Darden, D. York, L. Pedersen, Particle mesh Ewald: An N·log(N) method for Ewald sums in large systems, J. Chem. Phys. 98 (12) (1998) 10089–10092, https://doi.org/10.1063/1.464397.
[61] W.G. Hoover, Canonical dynamics: Equilibrium phase-space distributions, Phys. Rev. A 31 (3) (Mar. 1985) 1695–1697, https://doi.org/10.1103/PhysRevA.31.1695.
[62] I.F. Galván, M.L. Sánchez, M.E. Martín, F.J. Olivares del Valle, M.A. Aguilar, Geometry optimization of molecules in solution: Joint use of the mean field approximation and the free-energy gradient method, J. Chem. Phys. 118 (1) (2003) pp, https://doi.org/10.1063/1.1525798.
[63] N. Okuyama-Yoshida, M. Nagaoka, T. Yamabe, Transition-state optimization on free energy surface: Toward solution chemical reaction ergodography, Int. J. Quantum Chem., vol. 70, no. 1, 1998, doi: 10.1002/(SICI)1097-461X(1998)70:1<95::AID-QUA7>3.0.CO;2-0.
[64] N. Okuyama-Yoshida, K. Kataoka, M. Nagaoka, T. Yamabe, Structure optimization via free energy gradient method: application to glycine zwitterion in aqueous solution, J. Chem. Physic5 113 (9) (2000) 3519–3524, https://doi.org/10.1063/1.1287785.
[65] H. Hirao, Y. Nagae, M. Nagaoka, Transition-state optimization by the free energy gradient method: Application to aqueous-phase Menshutkin reaction between ammonia and methyl chloride, Chem. Phys. Lett. 348 (3–4) (Nov. 2001) 350–356, https://doi.org/10.1016/S0009-2614(01)01131-9.
[66] O. Tapia, Theoretical evaluation of solvent effects, Theor. Treat. Large Mol. Their Interact. (1991) 435–458, https://doi.org/10.1007/978-3-642-58183-0_11.
[67] J.G. Ángyán, Common theoretical framework for quantum chemical solvent effect theories, J. Math. Chem. 1991 101 10(1) (1992) 93–137, doi: 10.1007/BF01169172.
[68] P. Kollman, Free energy calculations: applications to chemical and biochemical phenomena, Chem. Rev. 93 (7) (1993) 2395–2417, https://doi.org/10.1021/CR00023A004.
[69] A.E. Mark, Free energy perturbation calculations, in: P.V.R. Schleyer, N.L. Allinger, T. Clark, J. Gasteiger, P.A. Kollman, H.F. Schaefer-III, P.R. Schreiner (Eds.), Encyclopedia of Computational Chemistry, vol. 2, Wiley and Sons, Chichester, 1998, pp. 1070–1083.
[70] A.M. Losa, I.F. Galván, M.A. Aguilar, M.E. Martín, A CASPT2//CASSCF study of vertical and adiabatic electron transitions of acrolein in water solution, J. Phys. Chem. B 111 (33) (2007) pp, https://doi.org/10.1021/jp071993r.
[71] B. Garrett, D. Truhlar, Additions and corrections - generalized transition state theory. quantum effects for collinear reactions of hydrogen molecules, J. Phys. Chem. 87(22) (1983) 4553–4553, doi: 10.1021/J100245A601.
[72] Y.Y. Chuang, D.G. Truhlar, Improved dual-level direct dynamics method for reaction rate calculations with inclusion of multidimensional tunneling effects and validation for the reaction of H with trans-N2H2, Chem. A Eur. J. 101 (20) (May 1997) 3808–3814, https://doi.org/10.1021/JP970052J/ASSET/IMAGES/MEDIUM/JP970052JE00021.GIF.
[73] J. Zheng et al., Polyrate, University of Minnesota, Minneapolis, 2017.
[74] R.L. Martin, Natural transition orbitals, J. Chem. Phys. 118 (11) (Feb. 2003) 4775, https://doi.org/10.1063/1.1558471.